


# Dynamics of charge equilibration and effects on producing neutron-rich isotopes around $N = 126$ in multinucleon transfer reactions

Zehong Liao,<sup>1</sup> Long Zhu<sup>1,\*</sup>, Jun Su,<sup>1</sup> and Cheng Li<sup>2</sup>

<sup>1</sup>*Sino-French Institute of Nuclear Engineering and Technology, Sun Yat-sen University, Zhuhai 519082, China*

<sup>2</sup>*College of Physics and Technology and Guangxi Key Laboratory of Nuclear Physics and Technology, Guangxi Normal University, Guilin 541004, China*

 (Received 7 July 2022; revised 31 December 2022; accepted 17 January 2023; published 24 January 2023)

The dynamics of the charge equilibration (CE) and the effects on the production of the neutron-rich isotopes around  $N = 126$  in multinucleon transfer reactions are still not well understood. In this work, we investigate the mechanism of the CE from different viewpoints by using the extended version of the dinuclear system model (DNS-sysu) and the improved quantum molecular dynamics (ImQMD) model. From the macroscopic and microscopic dynamical viewpoints, we find incomplete CE for the mass asymmetry reaction systems even in very deep collisions, and the behavior of “inverse CE” that the tendency of the fragments is away from the  $N/Z$  value of the compound system in the reaction  $^{140}\text{Xe} + ^{198}\text{Pt}$ . Unlike the slow process presented in the ImQMD model, the behavior of fast equilibration with the characteristic time  $\approx 0.52$  zs is obtained based on the DNS-sysu model, which is consistent with the experimental data. By performing a systematic calculation, the correlation between the CE and the mass asymmetry of the reaction systems is clarified, which not only accounts for the observed intriguing phenomena of the CE but also sheds light on the optimal combinations for producing the neutron-rich isotopes around  $N = 126$ .

DOI: [10.1103/PhysRevC.107.014614](https://doi.org/10.1103/PhysRevC.107.014614)

## I. INTRODUCTION

Because of the promised potential for producing exotic nuclei [1–13], the multinucleon transfer (MNT) process in massive nuclei collisions has attracted a lot of attention [14]. In particular, for producing neutron-rich heavy nuclei around  $N = 126$ , which are not only interesting for their nuclear structure but also contribute significantly to the understanding of the so called  $r$  process [15], the great advantages of the cross sections in the MNT reactions have been demonstrated [16–21].

Deep inelastic collisions (DICs) between nuclei in contact result in the profound reconstruction of the initial nuclei with the incident energy dissipation. The DICs at low energies show great potential to study the charge equilibration (CE) by tracking the differential motion of protons and neutrons [22]. The equilibration of neutron-to-proton ratios ( $N/Z$ ) that takes place at the early stage of the collision has been noticed [23–30]. Based on the time-dependent Hartree-Fock (TDHF) method, Simenel *et al.* compared the timescale for the CE and other processes, and indicated that the CE should not be the sole dissipation way [31]. On the other hand, several works have suggested that the CE is related to the quantum features, e.g., the giant dipole resonance (GDR) mode [32–34]. However, the interplay between equilibration and dissipation in quantum systems is still not well understood.

The difference in the  $N/Z$  of reaction partners influences the nucleon transfer direction and then the formation

probabilities of exotic fragments in the MNT process [35–37]. Moreover, inspired by the broad range of  $N/Z$  values, the developments of radioactive beam facilities around the world, such as FRIB (USA) [38], RIKEN (Japan) [39], SPIRAL2 (France) [40], and HIAF (China) [41], provide a great opportunity for getting deep insight into the mechanism of the CE and the favorable projectiles for producing exotic isotopes. The better understanding of CE will lead to more reliable predictions for producing neutron-rich isotopes around  $N = 126$  in MNT reactions.

In this work, the mechanism of the CE in the MNT reactions induced by Xe isotopes is studied by using the extended version of the dinuclear system model (DNS-sysu) and the improved quantum molecular dynamics (ImQMD) model. To interpret the CE behaviors and provide the essential information for producing  $N = 126$  neutron-rich isotopes in the MNT process, the correlations between the CE mode and the mass asymmetry  $\eta = (A_{\text{target}} - A_{\text{projectile}})/(A_{\text{target}} + A_{\text{projectile}})$  of the combinations are investigated in a systematic study.

## II. MODELS

The DNS-sysu model has been successfully used to describe MNT reactions [42–44]. In the DNS-sysu model, (1) the master equation is extended by introducing the dynamical deformation degree of freedom, (2) the temperature dependence of potential energy surface (PES) is involved, and (3) the unified description of fusion and MNT processes is achieved with the extension of the fusion concept [44]. In the DNS-sysu model, the production cross sections of the primary products with proton number  $Z_1$  and neutron number  $N_1$  can

\*Corresponding author: zhulong@mail.sysu.edu.cn

be calculated as follows:

$$\sigma_{\text{pr}}(Z_1, N_1, E_{\text{c.m.}}) = \frac{\pi \hbar^2}{2\mu E_{\text{c.m.}}} \sum_{J=0}^{J_{\text{max}}} (2J+1) T_{\text{cap}}(J, E_{\text{c.m.}}) \times \sum_{\beta_2} P(Z_1, N_1, \beta_2, J, E_{\text{c.m.}}, \tau_{\text{int}}) \times W_{\text{sur}}(Z_1, N_1, J, E^*), \quad (1)$$

where  $T_{\text{cap}}$  means the capture probability which is calculated with the Hill-Wheeler formula in the consideration of Coulomb barrier distribution. For heavy systems without potential pockets, the value of  $T_{\text{cap}}$  is estimated as 1 if the incident energy is above the interaction potential at the contact configuration.  $P$  is the distribution probability of the primary fragments with proton number  $Z_1$  and neutron number  $N_1$ .  $\beta_2$  is the dynamical deformation parameter of the DNS.  $W_{\text{sur}}$  is the deexcitation probability of the excited primary fragments. The contact time  $\tau_{\text{int}}$  can be calculated by the deflection function method [45,46].

The distribution probability  $P$  can be obtained by solving the master equations numerically with the corresponding potential energy surface, which can be written as [47]

$$\begin{aligned} & \frac{dP(Z_1, N_1, \beta_2, J, t)}{dt} \\ &= \sum_{Z'_1} W_{Z_1, N_1, \beta_2; Z'_1, N_1, \beta_2}(t) [d_{Z_1, N_1, \beta_2} P(Z'_1, N_1, \beta_2, J, t) \\ & \quad - d_{Z'_1, N_1, \beta_2} P(Z_1, N_1, \beta_2, J, t)] \\ & \quad + \sum_{N'_1} W_{Z_1, N_1, \beta_2; Z_1, N'_1, \beta_2}(t) [d_{Z_1, N_1, \beta_2} P(Z_1, N'_1, \beta_2, J, t) \\ & \quad - d_{Z_1, N'_1, \beta_2} P(Z_1, N_1, \beta_2, J, t)] \\ & \quad + \sum_{\beta'_2} W_{Z_1, N_1, \beta_2; Z_1, N_1, \beta'_2}(t) [d_{Z_1, N_1, \beta_2} P(Z_1, N_1, \beta'_2, J, t) \\ & \quad - d_{Z_1, N_1, \beta'_2} P(Z_1, N_1, \beta_2, J, t)], \end{aligned} \quad (2)$$

where  $W_{Z_1, N_1, \beta_2; Z'_1, N_1, \beta_2}$  denotes the mean transition probability from the channel  $(Z_1, N_1, \beta_2)$  to  $(Z'_1, N_1, \beta_2)$ , which is similar to  $N_1$  and  $\beta_2$ .  $d_{Z_1, N_1, \beta_2}$  is the microscopic dimension (the number of channels) corresponding to the macroscopic state  $(Z_1, N_1, \beta_2)$ . For the degrees of freedom of charge and neutron number, the sum is taken over all possible proton and neutron numbers that fragment 1 may take, but only one nucleon transfer is considered in the model ( $Z'_1 = Z_1 \pm 1$ ;  $N'_1 = N_1 \pm 1$ ). For the  $\beta_2$ , we take the range of  $-0.5$  to  $0.5$ . The evolution step length is  $0.01$ . The transition probability is related to the local excitation energy [48], in which the memory time is  $0.25\tau_0/A$ . Here,  $\tau_0 \equiv 2\pi\hbar/(1 \text{ MeV}) \approx 4 \times 10^{-21} \text{ s}$ , and  $A$  means the total nucleon number of the reaction [49].

The potential energy surface (PES) can be written as

$$\begin{aligned} U(Z_1, N_1, \beta_2, J, r = R_{\text{cont}}) &= \Delta(Z_1, N_1) + \Delta(Z_2, N_2) \\ & \quad + V(Z_1, N_1, \beta_2, J, r = R_{\text{cont}}) \\ & \quad + \frac{1}{2}C_1(\delta\beta_2^1)^2 + \frac{1}{2}C_2(\delta\beta_2^2)^2. \end{aligned} \quad (3)$$

TABLE I. The model parameters (IQ2) adopted in this work.

$\alpha$ (MeV)	$\beta$ (MeV)	$\gamma$	$g_{\text{sur}}$ (MeV fm <sup>2</sup> )	$g_{\tau}$ (MeV)	$\eta$	$C_s$ MeV	$\kappa_s$ (fm <sup>2</sup> )	$\rho_0$ (fm <sup>-3</sup> )
-356	303	7/6	7.0	12.5	2/3	32.0	0.08	0.165

Here,  $\Delta(Z_i, N_i)$  ( $i = 1, 2$ ) is the mass excess of the  $i$ th fragment [50]. The last two terms are the deformation energies which can be calculated using the methods shown in Refs. [47,51].  $R_{\text{cont}}$  is the position where the nucleon transfer process takes place [42].

The effective nucleus-nucleus interaction potential  $V$  consists of the long-range Coulomb repulsive potential, the attractive short-range nuclear potential, and the centrifugal potential:

$$V(Z_1, N_1, \beta_2, J, r) = V_{\text{N}}(Z_1, N_1, \beta_2, r) + V_{\text{C}}(Z_1, N_1, \beta_2, r) + \frac{(J\hbar)^2}{2\zeta_{\text{rel}}}. \quad (4)$$

where  $\zeta_{\text{rel}}$  is the moment of inertia for the relative motion of the DNS. More detailed descriptions of Coulomb potential  $V_{\text{C}}$  and nuclear potential  $V_{\text{N}}$  can be found in Refs. [52,53]. To systematically study the evolution of the CE, all reactions in this work are calculated and studied at 1.2 times interaction potential energies at the contact positions.

The ImQMD model [54] is an improved version of the quantum molecular dynamics model [55]. In this version, the Hamiltonian of the system is written as the sum of the kinetic energy  $T = \sum_i \frac{p_i^2}{2m_i}$  and effective interaction potential energy:

$$H = T + U_{\text{Coul}} + U_{\text{loc}}. \quad (5)$$

Here,  $U_{\text{Coul}}$  is the Coulomb interaction potential energy,

$$\begin{aligned} U_{\text{Coul}} &= \frac{1}{2} \iint \rho_p(\mathbf{r}) \frac{e^2}{|\mathbf{r} - \mathbf{r}'|} \rho_p(\mathbf{r}') d\mathbf{r} d\mathbf{r}' \\ & \quad - e^2 \frac{3}{4} \left(\frac{3}{\pi}\right)^{1/3} \int \rho_p^{4/3} d\mathbf{r}. \end{aligned} \quad (6)$$

with  $\rho_p$  the density distribution of protons of the system.  $U_{\text{loc}}$  is the nuclear interaction potential energy, which is obtained from the integration of the Skyrme energy density functional  $U_{\text{loc}} = \int V_{\text{loc}}(\mathbf{r}) d\mathbf{r}$  without the spin-orbit term. The nuclear interaction potential density  $V_{\text{loc}}$  can be written as

$$\begin{aligned} V_{\text{loc}} &= \frac{\alpha}{2} \frac{\rho^2}{\rho_0} + \frac{\beta}{\gamma+1} \frac{\rho^{\gamma+1}}{\rho_0^\gamma} + \frac{g_{\text{sur}}}{2\rho_0} (\nabla\rho)^2 \\ & \quad + \frac{C_s}{2\rho_0} [\rho^2 - \kappa_s (\nabla\rho)^2] \delta^2 + g_\tau \frac{\rho^{\eta+1}}{\rho_0^\eta}, \end{aligned} \quad (7)$$

where  $\delta$  is the isospin asymmetry. The parameters are shown in Table I. The density distribution in the coordinate space  $\rho(\mathbf{r})$  is given by

$$\rho(\mathbf{r}) = \sum_i \frac{1}{(2\pi\sigma_r^2)^{3/2}} \exp\left[-\frac{(\mathbf{r} - \mathbf{r}_i)^2}{2\sigma_r^2}\right], \quad (8)$$

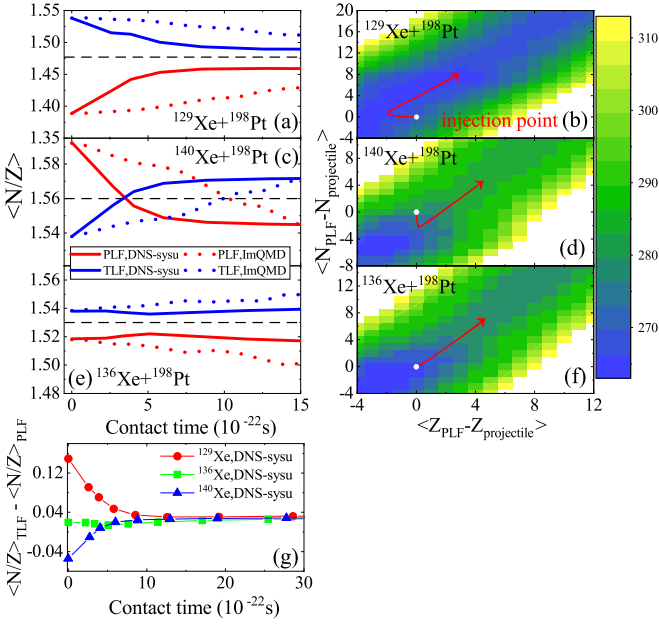


FIG. 1. Left panels: Calculated average  $N/Z$  values of the PLF and TLF in the reactions  $^{129}\text{Xe} + ^{198}\text{Pt}$  (a),  $^{140}\text{Xe} + ^{198}\text{Pt}$  (c), and  $^{136}\text{Xe} + ^{198}\text{Pt}$  (e) as a function of the contact time within the DNS-sysu and ImQMD models. The  $N/Z$  values of compound systems are also shown with the black horizontal dashed lines. Right panels: Contour plots of the PES (in MeV) with the drift trajectories of the first moments of PLF distributions in the  $(\langle Z_{\text{PLF}} - Z_{\text{Projectile}} \rangle, \langle N_{\text{PLF}} - N_{\text{Projectile}} \rangle)$  plane for the reactions  $^{129}\text{Xe} + ^{198}\text{Pt}$  (b),  $^{140}\text{Xe} + ^{198}\text{Pt}$  (d), and  $^{136}\text{Xe} + ^{198}\text{Pt}$  (f). (g) The discrepancies of average  $N/Z$  values between the TLF and PLF as a function of the interaction time calculated in the DNS-sysu model for the reactions  $^{129}\text{Xe}$ ,  $^{136}\text{Xe}$ ,  $^{140}\text{Xe} + ^{198}\text{Pt}$ . The incident energies  $E_{\text{c.m.}} = 470, 476$ , and  $466$  MeV for the reactions induced by  $^{129, 136, 140}\text{Xe}$ .

where  $\sigma_r$  is the Gaussian wave packet variation. The IQ2 parameter sets (see in Table I) are adopted in this work. The fermionic nature in ImQMD is treated as the method proposed by Papa *et al* [56]. In MNT reactions, the total kinetic energy-mass distributions of the primary binary fragments in different contact time ranges [57] or impact parameters [58] can serve as an effective basis for classifying different channels. The exotic fragments or specific objective nuclei could be produced in the channels of deep-inelastic collisions, quasifission, and quasielastic collisions. Therefore, the events from central collisions to grazing are considered in this work. To get the production cross sections of the final products after the deexcitation process, the code GEMINI++ [59] is used to treat the deexcitation process of primary fragments. Subsequent de-excitation cascades of the excited fragments via emission of light particles (neutron, proton,  $\alpha$ , etc.) and  $\gamma$  rays competing with the fission process leads to the final mass distribution of the reaction products.

### III. RESULTS AND DISCUSSIONS

To clarify the  $N/Z$  asymmetry effect in MNT reactions, Fig. 1(a) shows the average  $N/Z$  values of the projectilelike

fragments (PLF) and targetlike fragments (TLF) as a function of the contact time in the reaction  $^{129}\text{Xe} + ^{198}\text{Pt}$  within the framework of the DNS-sysu model. The large discrepancy of  $N/Z$  values between  $^{129}\text{Xe}$  and  $^{198}\text{Pt}$ , e.g.,  $N/Z = 1.39$  for  $^{129}\text{Xe}$ ,  $N/Z = 1.54$  for  $^{198}\text{Pt}$ , is expected to confirm the presence of CE behaviors. One interesting behavior can be seen: the average  $N/Z$  values of the PLF and TLF trend toward the  $N/Z$  value of the compound system ( $N/Z = 1.48$ ) but do not lead to being identical even in very deep collisions. We also show the results from the ImQMD model. Incomplete CE is also noticed. Besides, unlike the results from the DNS-sysu model, the CE takes place at the whole collision stage gradually.

In principle, the MNT process can be described as the reaction upon the so-called PES, where the dynamical evolution of a dinuclear system can be treated as the process of exchanging the independent particles between the nuclei [60]. Plotted in Figs. 1(b), 1(d), and 1(f), the PES can be defined as the contour of the first moments of the PLF distributions, i.e.,  $(\langle Z_{\text{PLF}} - Z_{\text{Projectile}} \rangle, \langle N_{\text{PLF}} - N_{\text{Projectile}} \rangle)$ . Taking the reaction  $^{129}\text{Xe} + ^{198}\text{Pt}$  in Fig. 1(b) as an example, the trajectory starts from the injection point and relaxes to the valley of the PES driven by the PES gradient [see the red line in Fig. 1(b)], which indicates that the projectile tends to lose protons and absorb neutrons from the target.

In Fig. 1(c), we also show the results of the reaction  $^{140}\text{Xe} + ^{198}\text{Pt}$ . The  $N/Z$  value of the projectile  $^{140}\text{Xe}$  is 1.59, which is larger than that of the target. However, unlike the reaction  $^{129}\text{Xe} + ^{198}\text{Pt}$ , the inverse relationship ( $N/Z_{\text{PLF}} < N/Z_{\text{TLF}}$ ) is noticed during the evolution. Similar behavior is also apparent from the ImQMD calculations, except the crossover appears at a quite delayed contact time. The transfer of neutrons from  $^{140}\text{Xe}$  to  $^{198}\text{Pt}$  is promoted, due to negative values of  $\Delta U$  in the neutron stripping channels, such as  $\Delta U_{-1n} = -2.6$  MeV,  $\Delta U_{-2n} = -4.8$  MeV, and  $\Delta U_{-3n} = -6.8$  MeV. Here,  $\Delta U_{-xn} [= U(Z_p, N_p - x, \beta_2 = 0, J = 0, r = R_{\text{cont}}) - U(Z_p, N_p, \beta_2 = 0, J = 0, r = R_{\text{cont}})]$  represents the driving potential needed to be overcome in the neutron transfer process. A detailed description of  $U$  is shown in Eq. (3). The system  $^{140}\text{Xe} + ^{198}\text{Pt}$  with negative values of  $\Delta U_{-xn}$  tends to enhance the average  $N/Z$  values of the TLF and decrease those of the PLF.

Compared with the initial entrance channel, the behavior called “inverse CE,” producing the fragments with the average  $N/Z$  values farther from the  $N/Z$  value of the compound system ( $N/Z = 1.56$ ), is noticed. This is a strong indication that the underlying mechanism behind the CE does not only depend on the  $N/Z$  asymmetry in the entrance channel.

Furthermore, considering the different initial  $N/Z$  values for the projectile and target in the reaction  $^{136}\text{Xe} + ^{198}\text{Pt}$  ( $N/Z = 1.52$  for  $^{136}\text{Xe}$ ,  $N/Z = 1.54$  for  $^{198}\text{Pt}$ ), the behavior of CE should also be noticed on some levels. However, as shown in Fig. 1(e), the almost flat variation of the average  $N/Z$  values with the interaction time is presented in both the DNS-sysu and ImQMD model calculations. The PES of the reaction  $^{136}\text{Xe} + ^{198}\text{Pt}$  is shown in Fig. 1(f). Since the trajectory sticks to the bottom of the valley, the weak variation of the average  $N/Z$  values can be explained.

To compare the above systems, in Fig. 1(g), we show the differences between the average  $N/Z$  values of the TLF and PLF ( $\langle N/Z \rangle_{\text{TLF}} - \langle N/Z \rangle_{\text{PLF}}$ ) as a function of the interaction time calculated in the DNS-sysu model for the reactions  $^{129,136,140}\text{Xe} + ^{198}\text{Pt}$ . It is interesting to see that for all three systems the values of  $\langle N/Z \rangle_{\text{TLF}} - \langle N/Z \rangle_{\text{PLF}}$  evolve to a saturation value of 0.04, rather than 0.

From the equilibration perspective timescale, the CE process is believed to be the fastest one among all the equilibration modes [61]. To compare the equilibration timescale of various systems, we introduce a general “normalized” observable  $\delta I(t) = [I(t) - I_\infty]/(I_0 - I_\infty)$  [31]. Here,  $I_0$  and  $I_\infty$  respectively denote the initial and expected saturation  $N/Z$  values of the projectile. During the evolution, it is reasonable to see that the  $\delta I$  decays from 1 to 0. The so-called characteristic time  $\tau$  can be adopted to characterize the CE process, which is the parameter denoting the decay of  $\delta I$  following  $\delta I = y_0 + A_0 \exp(-t/\tau)$ .

In Fig. 2(a), several systems are calculated to present a comprehensive timescale of the CE in this work. The incident energy of  $E_{\text{c.m.}} = 1.2V(r = R_{\text{cont}})$  is used for each reaction. The values of  $V(r = R_{\text{cont}})$  are 143, 276, 423, 439, 573, 650, and 618 MeV, respectively, for the reactions  $^{58}\text{Ni} + ^{124}\text{Sn}$ ,  $^{92}\text{Kr} + ^{208}\text{Pb}$ ,  $^{112}\text{Sn} + ^{238}\text{U}$ ,  $^{118}\text{Xe} + ^{238}\text{U}$ ,  $^{186}\text{W} + ^{238}\text{U}$ ,  $^{196}\text{Hg} + ^{239}\text{Pu}$ , and  $^{198}\text{Pt} + ^{238}\text{U}$ . Despite the fluctuations, all systems exhibit a similar and fast decay pattern. By fitting the data in the above reactions, 0.52 zs for the characteristic time  $\tau$  is obtained in this work (red line), which is in the same order of magnitude as the experimental data ( $\tau \approx 0.3$  zs) in Ref. [25], the measurement ( $\tau \approx 0.14$  zs) by Kratz *et al.* [23], and 0.5 zs from the TDHF calculations [26]. Applying the microscopic stochastic mean-field approach [28], Ayik *et al.* performed a similar CE calculation. The system reaches equilibrium after 1 zs from first touching, which is also consistent with the result in this work.

Furthermore, seen from Fig. 1, the average  $N/Z$  values of PLF or TLF, estimated based on the DNS-sysu and ImQMD models, show quite a different trend with contact time elapsed. The slow CE process shown in the ImQMD model might be due to the absence of the spin-orbit coupling in the interaction and the details of the Pauli blocking treatment [62,63].

The shell effects on the CE are also investigated in the reactions  $^{78}\text{Kr} + ^{208}\text{Pb}$  and  $^{129}\text{Xe} + ^{198}\text{Pt}$  within the DNS-sysu model at  $E_{\text{c.m.}} = 347$  and 470 MeV, respectively. Note that the characteristic time extracted from the reaction  $^{78}\text{Kr} + ^{208}\text{Pb}$  with shell corrections (0.31 zs) is greater than that without shell corrections (0.22 zs). The delayed CE is because the nucleon transfer process would be inhibited due to the doubly magic  $^{208}\text{Pb}$  target. However, an enhancement of the shell effects in the equilibrium speed can be observed in the reaction  $^{129}\text{Xe} + ^{198}\text{Pt}$  ( $\tau_{\text{with-shell}} \approx 0.27$  zs,  $\tau_{\text{without-shell}} \approx 0.38$  zs). This enhancement can be attributed to the attraction of the proton shell closure  $Z = 82$  for transferring protons from  $^{129}\text{Xe}$  to  $^{198}\text{Pt}$ . In addition, the phenomenon that  $^{129}\text{Xe}$  is preferably driven to lost protons by the PES gradient can also be seen clearly in Fig. 1(d). As we can see, for each reaction, our calculations demonstrate that the shell effects could influence the neutron and proton flow strongly. In Fig. 2(c),

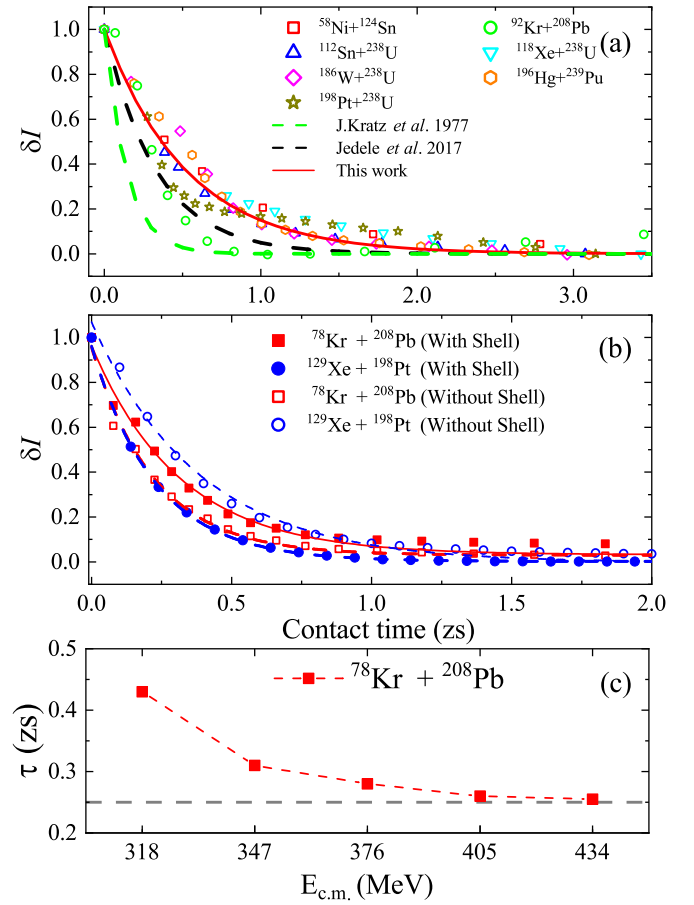


FIG. 2. (a) The evolution degree of the CE [ $\delta I(t)$ ] as a function of contact time from DNS-sysu calculation of the reactions  $^{58}\text{Ni} + ^{124}\text{Sn}$ ,  $^{92}\text{Kr} + ^{208}\text{Pb}$ ,  $^{112}\text{Sn} + ^{238}\text{U}$ ,  $^{118}\text{Xe} + ^{238}\text{U}$ ,  $^{186}\text{W} + ^{238}\text{U}$ ,  $^{196}\text{Hg} + ^{239}\text{Pu}$ , and  $^{198}\text{Pt} + ^{238}\text{U}$ . The green and black dashed lines show the expected equilibration, assuming the rate constants of 0.14 zs reported experimentally by Kratz *et al.* [23] and 0.3 zs reported experimentally by Jedelev *et al.* [25], respectively. (b) Evolution of  $\delta I$  as a function of contact time from DNS-sysu calculations of  $^{78}\text{Kr} + ^{208}\text{Pb}$  (squares) and  $^{129}\text{Xe} + ^{198}\text{Pt}$  (circles). The solid symbols and open symbols denote the results with and without shell corrections, respectively. The solid line and dashed line denote the expected fitting results with and without shell corrections, respectively. (c) The CE characteristic time  $\tau$  as a function of the incident energy for the reaction  $^{78}\text{Kr} + ^{208}\text{Pb}$  calculated in the DNS-sysu model. The horizontal dashed line is used to guide the eye.

we show the CE characteristic time  $\tau$  as a function of the incident energy. Interestingly,  $\tau$  gradually decreases with the increase of incident energy and reaches saturation for incident energy higher than 405 MeV [ $1.4V(r = R_{\text{cont}})$ ]. The high incident energy enhances the energy dissipating into the interior of the system, which promotes the process of equilibration. However, the timescale of equilibrium shows a limit, which can be roughly estimated by dividing the size of a nucleus by the speed at which isospin waves or nucleons propagate. Note that the absence of microscopic characteristics prevents using the DNS model to further investigate the CE process from the viewpoint of quantal fluctuation, which might play an important role in the fast CE process.



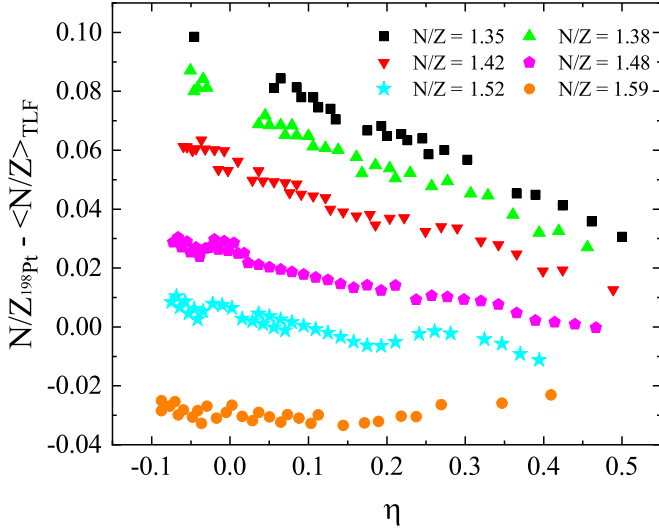


FIG. 3. The values of  $N/Z_{198\text{Pt}} - \langle N/Z \rangle_{\text{TLF}}$  in MNT reactions with the target  $^{198}\text{Pt}$  as a function of the mass asymmetry of combinations and  $N/Z$  values of the projectiles. The projectiles are selected based on the  $N/Z$  values, which are about 1.35, 1.38, 1.42, 1.48, 1.52, and 1.59.

Due to the “curvature” of the  $\beta$ -stability line, the heavy nuclei show the capability of possessing more neutrons than the light ones, which could affect the nucleon flow in the collisions. The CE would be strongly affected by the mass asymmetry of the reaction partners. Therefore, to clarify the interesting phenomena shown in Fig. 1, one conjecture can be made that the initial mass asymmetry of combinations also plays a significant role during the isospin transfer process.

To investigate the correlations between the CE and the mass asymmetry of the colliding combinations, reactions with projectiles spanning a broad range of masses and  $N/Z$  values bombarding the target  $^{198}\text{Pt}$  are systematically studied. In Fig. 3, we show the values of  $N/Z_{198\text{Pt}} - \langle N/Z \rangle_{\text{TLF}}$  as a function of the mass asymmetry of colliding combinations and the  $N/Z$  values of the projectiles. Each symbol denotes a reaction system with specific  $N/Z$  asymmetry and mass asymmetry. Despite the minor fluctuations, a correlation between the mass asymmetry and the  $N/Z$  asymmetry is clearly shown to influence the neutron richness of the TLF.

As shown in Fig. 3, for the case of  $N/Z = 1.35$ , the TLF neutron richness strongly depends on the mass asymmetries of the colliding systems. One can see that the combinations with positive large values of  $\eta$  show small discrepancies between the average  $N/Z$  values of TLF and that of  $^{198}\text{Pt}$ , although the systems present large  $N/Z$  asymmetries. The same behavior can be seen for the projectiles with  $N/Z = 1.59$  (shown as brown circles) which is higher than 1.54 of  $^{198}\text{Pt}$ . This behavior supports the conjecture we made that the mass asymmetries of the reaction combinations strongly affect the CE process. Furthermore, it can be seen that the mass asymmetry dependence of CE is weakened for the  $N/Z$  symmetric combinations. For example, for the reactions induced by projectiles with  $N/Z$  values close to 1.52 (shown

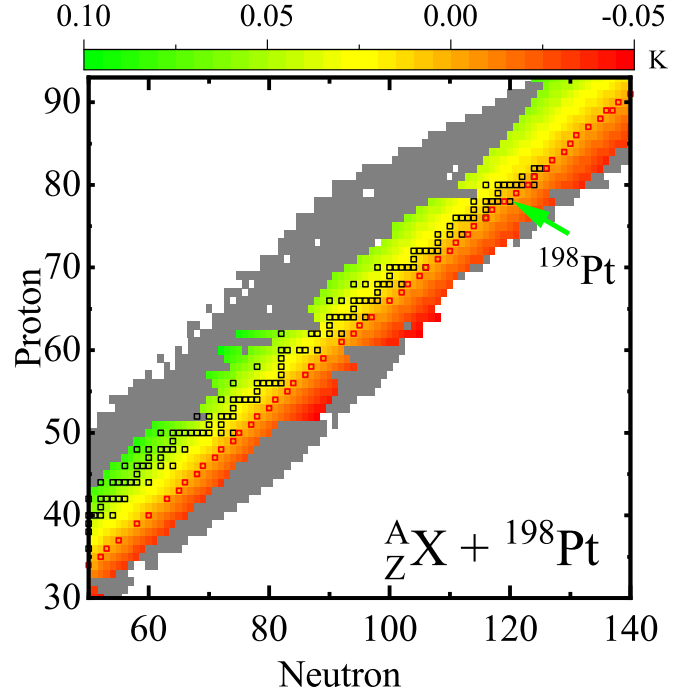


FIG. 4. The factor  $K$  for the reactions based on  $^{198}\text{Pt}$  target as a function of the neutron and proton numbers of the projectiles. The black open squares show nuclides along the  $\beta$ -stability line. The red open squares denote the reactions with  $K$  values that are approximately equal to 0.

as blue stars), the weak variation of  $N/Z_{198\text{Pt}} - \langle N/Z \rangle_{\text{TLF}}$  values with the mass asymmetry can be seen. This is the main reason for the behavior shown in Fig. 1(e). Therefore, the intriguing phenomena shown in Fig. 1, such as incomplete CE and “inverse CE,” are mainly because of the correlation between the CE and the mass asymmetry. Here, we point out that the complete CE is hard reach in mass asymmetric systems.

As stated above, the evolution of the CE can be influenced by the  $N/Z$  asymmetry and the initial mass asymmetry. To further understand the effect of the CE process in MNT reactions for producing neutron-rich isotopes and provide guidance for selecting favorable combinations, we define a relative isospin flow factor  $K$ , which can be written as

$$K = \frac{(N/Z)_{\text{target}} - \langle N/Z \rangle_{\text{TLF}}}{(N/Z)_{\text{CN}}}. \quad (9)$$

The negative values of  $K$  denote that there are advantages for producing neutron-rich TLF. In contrast, for positive values of  $K$ , the corresponding projectiles could enhance the probabilities of producing neutron-deficient TLF. For example, for the reactions  $^{129,136,140}\text{Xe} + ^{198}\text{Pt}$  we studied above, the corresponding values of the factor  $K$  are 0.034, 0, and 0.02, respectively. Note that the value of the factor  $K$  could sensitively reveal the isospin flow directions in different reactions. We systematically investigate the  $K$  values in the reactions based on the  $^{198}\text{Pt}$  target. In Fig. 4, we show the distribution of the factor  $K$  as a function of the neutron and proton numbers of the projectiles. The red open squares denote the

reactions for which  $K$  values are approximately equal to 0. In other words, for the reactions to the “northwest” of these red open squares in the chart, the average  $N/Z$  values of the TLF are less than 1.54 of the  $^{198}\text{Pt}$  target. In contrast, the average  $N/Z$  values of TLF are greater than 1.54 of the  $^{198}\text{Pt}$  target for the reactions to the “southeast” of the red open squares. For the reactions farther away from these red open squares, more neutron-rich or neutron-deficient TLF could be produced. The black open squares denote reactions with the projectiles along the  $\beta$ -stability line. For the regions with  $Z < 50$  and  $N < 80$ , we notice that the red open squares are located on the more neutron-rich side of the  $\beta$ -stability line. Hence, only extremely neutron-rich projectiles in this region could promote the production of the neutron-rich TLF. On the other hand, for the reactions with heavy projectiles, such as the mass symmetric reactions, it can be seen obviously that these red open squares are close to the  $\beta$ -stability line. It is worth mentioning that beams of nuclides around the  $\beta$ -stability line usually show higher intensities compared to those far from  $\beta$  stability. Therefore, reactions induced by heavy projectiles would be efficient for producing neutron-rich nuclei around  $N = 126$ .

In order to optimize the reaction combinations for producing unknown neutron-rich nuclei, the reactions  $^{129}\text{Xe} + ^{198}\text{Pt}$ ,  $^{136}\text{Xe} + ^{198}\text{Pt}$ ,  $^{140}\text{Xe} + ^{198}\text{Pt}$ ,  $^{202}\text{Pt} + ^{198}\text{Pt}$  and  $^{238}\text{U} + ^{198}\text{Pt}$  are investigated at incident energies of  $E_{\text{c.m.}} = 470, 476, 466, 663, \text{ and } 741 \text{ MeV}$ , respectively. In Fig. 5(a), we show the calculated production cross sections for  $N = 126$  isotones with  $Z < 80$  produced in the reactions  $^{129,136,140}\text{Xe} + ^{198}\text{Pt}$ . As we expected, the reactions induced by projectiles with high neutron richness ( $N/Z \approx 1.59$  for  $^{140}\text{Xe}$ ) show great advantages of cross sections for producing neutron-rich nuclei. This can be interpreted by the intense CE caused by the large  $N/Z$  asymmetry. We also extract the cross sections of the primary fragments in the proton pickup channels for the reactions  $^{140}\text{Xe} + ^{198}\text{Pt}$ ,  $^{202}\text{Pt} + ^{198}\text{Pt}$ , and  $^{238}\text{U} + ^{198}\text{Pt}$  shown in Figs. 5(b)–5(e). It can be seen that the production cross sections of the neutron-rich nuclei in the reaction induced by  $^{140}\text{Xe}$  are lower than those in the  $^{202}\text{Pt}$  and  $^{238}\text{U}$  induced ones, although  $^{140}\text{Xe}$  has an even larger  $N/Z$  value. This is because the  $^{140}\text{Xe} + ^{198}\text{Pt}$  reaction presents the positive large value of  $\eta$  and the CE is inhibited, just like the correlation behaviors between  $\eta$  and the CE process we discussed above. On the other side, the saturation values of  $\langle N/Z \rangle_{\text{TLF}} - \langle N/Z \rangle_{\text{PLF}}$  for the reactions  $^{238}\text{U} + ^{198}\text{Pt}$  and  $^{202}\text{Pt} + ^{198}\text{Pt}$  are 0.01 and 0, respectively, which are close to the complete CE status. We know that, to choose optimal combinations, the beam intensity should be considered. Compared with the radioactive nuclides  $^{202}\text{Pt}$  and  $^{140}\text{Xe}$ , the  $^{238}\text{U}$  induced reaction is a better candidate for producing neutron-rich nuclei around  $N = 126$ .

#### IV. CONCLUSIONS

The mechanism of the CE is investigated within the DNS-sysu (macroscopic approach) and ImQMD (microscopic dynamical approach) models. It is found that the two models show different equilibration characteristic times. For the DNS-sysu model, it is noticed that the CE occurs at the early

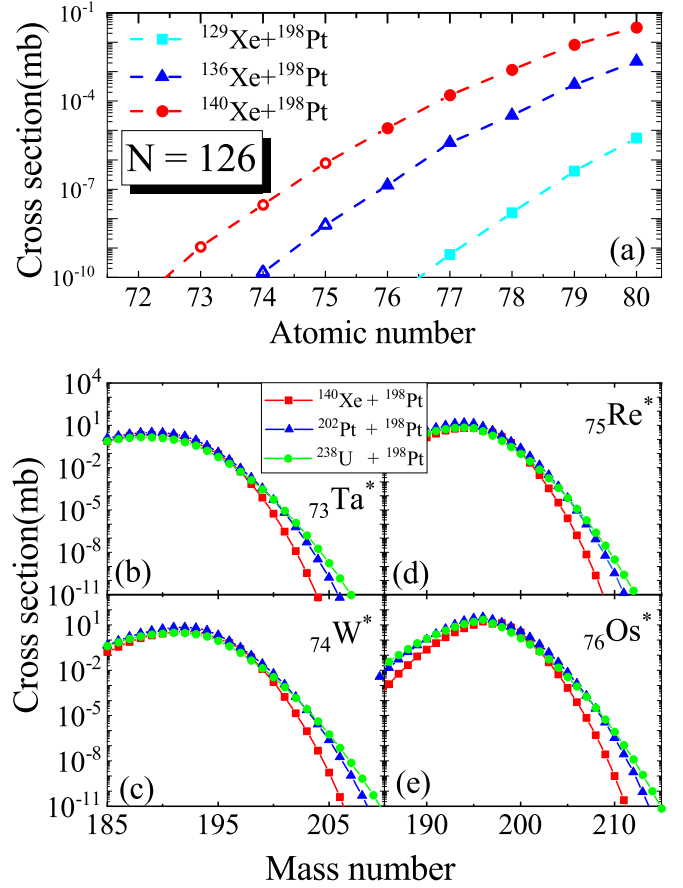


FIG. 5. (a) Calculated production cross sections of the  $N = 126$  isotones in the MNT reactions  $^{129}\text{Xe}$ ,  $^{136}\text{Xe}$ , and  $^{140}\text{Xe} + ^{198}\text{Pt}$  within the DNS-sysu model with GEMINI++ code. Open symbols denote unknown nuclei. (b)–(e) The calculated production cross sections of the primary fragments in  $^{140}\text{Xe} + ^{198}\text{Pt}$ ,  $^{202}\text{Pt} + ^{198}\text{Pt}$ , and  $^{238}\text{U} + ^{198}\text{Pt}$ .

stage of the colliding. The equilibration characteristic time in the DNS-sysu model is about 0.52 zs, in the same order of magnitude as the experimental data (0.3 zs) in Ref. [25], and the TDHF calculations (0.5 zs). However, the ImQMD calculations show that the equilibration is a slow process and takes place in the whole colliding process. In addition, the shell effect on CE is studied based on the reactions  $^{78}\text{Kr} + ^{208}\text{Pb}$  and  $^{129}\text{Xe} + ^{198}\text{Pt}$  within the DNS-sysu model. The obvious influence of shell closures and incident energy on CE characteristic time is noticed. In both the DNS-sysu and ImQMD calculations, it is found that (i) the complete CE is hard reach in the mass asymmetric reaction systems and (ii) “inverse CE” takes place in the reaction  $^{140}\text{Xe} + ^{198}\text{Pt}$ . In this work, by performing a systematic calculation, for the first time the correlations between the CE and the mass asymmetry of the reaction systems are clarified, and the above intriguing CE behaviors are interpreted with superposition of the mass asymmetry and the charge asymmetry of the colliding combinations.

With the definition of the relative isospin flow factor  $K$ , the isospin flow in  $^{198}\text{Pt}$  target-based reactions with different colliding partners is investigated systematically. It is found

that light projectiles are not good candidates for producing neutron-rich isotopes  $N = 126$  when considering isospin flow and relatively low beam intensities. Besides, the results in this work suggest that the combination  $^{238}\text{U} + ^{198}\text{Pt}$  is favorable for producing unknown  $N = 126$  isotopes.

## ACKNOWLEDGMENTS

L.Z. thanks Dr. P. W. Wen, H. H. Wen, and S. L. Chen for their careful reading of the manuscript. This work was supported by the National Natural Science Foundation of China under Grants No. 12075327 and No. 11875328.

- [1] L. Zhu, C. Li, C.-C. Guo, J. Su, P.-W. Wen, G. Zhang, and F.-S. Zhang, Theoretical progress on production of isotopes in the multinucleon transfer process, *Int. J. Mod. Phys. E* **29**, 2030004 (2020).
- [2] F.-S. Zhang, C. Li, L. Zhu, and P.-W. Wen, Production cross sections for exotic nuclei with multinucleon transfer reactions, *Front. Phys.* **13**, 132113 (2018).
- [3] L. Corradi, S. Szilner, G. Pollaro, D. Montanari, E. Fioretto, A. Stefanini, J. Valiente-Dobón, E. Farnea, C. Michelagnoli, G. Montagnoli *et al.*, Multinucleon transfer reactions: Present status and perspectives, *Nucl. Instrum. Methods Phys. Res. Sect. B* **317**, 743 (2013).
- [4] W. D. Loveland, The synthesis of new neutron-rich heavy nuclei, *Front. Phys.* **7**, 23 (2019).
- [5] G. Adamian, N. Antonenko, A. Diaz-Torres, and S. Heinz, How to extend the chart of nuclides? *Eur. Phys. J. A* **56**, 47 (2020).
- [6] K. Sekizawa, TDHF theory and its extensions for the multinucleon transfer reaction: A mini review, *Front. Phys.* **7**, 20 (2019).
- [7] C. Li, F. Zhang, J. Li, L. Zhu, J. Tian, N. Wang, and F.-S. Zhang, Multinucleon transfer in the  $^{136}\text{Xe} + ^{208}\text{Pb}$  reaction, *Phys. Rev. C* **93**, 014618 (2016).
- [8] Z. Wu and L. Guo, Microscopic studies of production cross sections in multinucleon transfer reaction  $^{58}\text{Ni} + ^{124}\text{Sn}$ , *Phys. Rev. C* **100**, 014612 (2019).
- [9] W. Krolas, R. Broda, B. Fornal, T. Pawlat, H. Grawe, K. Maier, M. Schramm, and R. Schubart, Gamma coincidence study of  $^{208}\text{Pb} + 350\text{ MeV } ^{64}\text{Ni}$  collisions, *Nucl. Phys. A* **724**, 289 (2003).
- [10] A. C. Mignerey, V. E. Viola, Jr., H. Breuer, K. L. Wolf, B. G. Glagola, J. R. Birkelund, D. Hilscher, J. R. Huizenga, W. U. Schröder, and W. W. Wilcke, Dependence of Isobaric Charge Distributions on Energy Loss and Mass Asymmetry in Damped Collisions, *Phys. Rev. Lett.* **45**, 509 (1980).
- [11] P. Wen, A. Nasirov, C. Lin, and H. Jia, Multinucleon transfer reaction from view point of dynamical dinuclear system method, *J. Phys. G: Nucl. Part. Phys.* **47**, 075106 (2020).
- [12] V. I. Zagrebaev and W. Greiner, Production of heavy and super-heavy neutron-rich nuclei in transfer reactions, *Phys. Rev. C* **83**, 044618 (2011).
- [13] V. Saiko and A. Karpov, Multinucleon transfer as a method for production of new heavy neutron-enriched isotopes of transuranium elements, *Eur. Phys. J. A* **58**, 41 (2022).
- [14] V. V. Volkov, Deep inelastic transfer reactions—the new type of reactions between complex nuclei, *Phys. Rep.* **44**, 93 (1978).
- [15] H. Grawe, K. Langanke, and G. Martínez-Pinedo, Nuclear structure and astrophysics, *Rep. Prog. Phys.* **70**, 1525 (2007).
- [16] V. Zagrebaev and W. Greiner, Production of New Heavy Isotopes in Low-Energy Multinucleon Transfer Reactions, *Phys. Rev. Lett.* **101**, 122701 (2008).
- [17] Y. X. Watanabe, Y. H. Kim, S. C. Jeong, Y. Hirayama, N. Imai, H. Ishiyama, H. S. Jung, H. Miyatake, S. Choi, J. S. Song, E. Clement, G. deFrance, A. Navin, M. Rejmund, C. chmitt, G. Pollaro, L. Corradi, E. Fioretto, D. Montanari, M. Niikura, D. Suzuki, H. Nishibata, and J. Takatsu, Pathway for the Production of Neutron-Rich Isotopes around the  $N = 126$  Shell Closure, *Phys. Rev. Lett.* **115**, 172503 (2015).
- [18] J. S. Barrett, W. Loveland, R. Yanez, S. Zhu, A. D. Ayangeakaa, M. P. Carpenter, J. P. Greene, R. V. F. Janssens, T. Lauritsen, E. A. McCutchan, A. A. Sonzogni, C. J. Chiara, J. L. Harker, and W. B. Walters,  $^{136}\text{Xe} + ^{208}\text{Pb}$  reaction: A test of models of multinucleon transfer reactions, *Phys. Rev. C* **91**, 064615 (2015).
- [19] E. M. Kozulin, E. Vardaci, G. N. Knyazheva, A. A. Bogachev, S. N. Dmitriev, I. M. Itkis, M. G. Itkis, A. G. Knyazev, T. A. Loktev, K. V. Novikov, E. A. Razinkov, O. V. Rudakov, S. V. Smirnov, W. Trzaska, and V. I. Zagrebaev, Mass distributions of the system  $^{136}\text{Xe} + ^{208}\text{Pb}$  at laboratory energies around the coulomb barrier: A candidate reaction for the production of neutron-rich nuclei at  $n = 126$ , *Phys. Rev. C* **86**, 044611 (2012).
- [20] S. Heinz and O. Beliuskina, Deep inelastic transfer reactions—a new way to exotic nuclei? *J. Phys. Conf. Ser.* **515**, 012007 (2014).
- [21] O. Beliuskina, S. Heinz, V. Zagrebaev, V. Comas, C. Heinz, S. Hofmann, R. Knöbel, M. Stahl, D. Ackermann, F. Heßberger *et al.*, On the synthesis of neutron-rich isotopes along the  $N = 126$  shell in multinucleon transfer reactions, *Eur. Phys. J. A* **50**, 161 (2014).
- [22] A. B. McIntosh and S. J. Yennello, Interplay of neutron–proton equilibration and nuclear dynamics, *Prog. Part. Nucl. Phys.* **108**, 103707 (2019).
- [23] J. V. Kratz, H. Ahrens, W. Bögl, W. Brüche, G. Franz, M. Schädel, I. Warnecke, G. Wirth, G. Klein, and M. Weis, Charge-Asymmetry Equilibration in the Reaction of  $^{129,132,136}\text{Xe}$  with  $^{197}\text{Au}$  near the Interaction Barrier, *Phys. Rev. Lett.* **39**, 984 (1977).
- [24] E. Hernandez, W. Myers, J. Randrup, and B. Remaud, Quantal dynamics of charge equilibration in damped nuclear collisions, *Nucl. Phys. A* **361**, 483 (1981).
- [25] A. Jede, A. B. McIntosh, K. Hagel, M. Huang, L. Heilborn, Z. Kohley, L. W. May, E. McCleskey, M. Youngs, A. Zarrella, and S. J. Yennello, Characterizing Neutron-Proton Equilibration in Nuclear Reactions with Subzeptosecond Resolution, *Phys. Rev. Lett.* **118**, 062501 (2017).
- [26] A. S. Umar, C. Simenel, and W. Ye, Transport properties of isospin asymmetric nuclear matter using the time-dependent Hartree-Fock method, *Phys. Rev. C* **96**, 024625 (2017).
- [27] C. Simenel, D. Hinde, R. du Rietz, M. Dasgupta, M. Evers, C. Lin, D. Luong, and A. Wakhle, Influence of entrance-channel magicity and isospin on quasi-fission, *Phys. Lett. B* **710**, 607 (2012).
- [28] S. Ayik, M. Arik, E. C. Karanfil, O. Yilmaz, B. Yilmaz, and A. S. Umar, Quantal diffusion description of isotope production via the multinucleon transfer mechanism in  $^{48}\text{Ca} + ^{238}\text{U}$  collisions, *Phys. Rev. C* **104**, 054614 (2021).

- [29] K. Sekizawa and S. Ayik, Quantal diffusion approach for multinucleon transfer processes in the  $^{58,64}\text{Ni} + ^{208}\text{Pb}$  reactions: Toward the production of unknown neutron-rich nuclei, *Phys. Rev. C* **102**, 014620 (2020).
- [30] V. Saiko and A. Karpov, Role of charge equilibration in multinucleon transfer reactions, *Bull. Russ. Acad. Sci.: Phys.* **84**, 436 (2020).
- [31] C. Simenel, K. Godbey, and A. S. Umar, Timescales of Quantum Equilibration, Dissipation and Fluctuation in Nuclear Collisions, *Phys. Rev. Lett.* **124**, 212504 (2020).
- [32] C. Simenel, P. Chomaz, and G. de France, Quantum Calculation of the Dipole Excitation in Fusion Reactions, *Phys. Rev. Lett.* **86**, 2971 (2001).
- [33] V. Baran, D. M. Brink, M. Colonna, and M. Di Toro, Collective Dipole Bremsstrahlung in Fusion Reactions, *Phys. Rev. Lett.* **87**, 182501 (2001).
- [34] Y. Iwata, T. Otsuka, J. A. Maruhn, and N. Itagaki, Suppression of Charge Equilibration Leading to the Synthesis of Exotic Nuclei, *Phys. Rev. Lett.* **104**, 252501 (2010).
- [35] A. N. Andreyev, K. Nishio, and K.-H. Schmidt, Nuclear fission: A review of experimental advances and phenomenology, *Rep. Prog. Phys.* **81**, 016301 (2018).
- [36] X. J. Bao, S. Q. Guo, J. Q. Li, and H. F. Zhang, Influence of neutron excess of projectile on multinucleon transfer reactions, *Phys. Lett. B* **785**, 221 (2018).
- [37] L. Zhu, J. Su, W.-J. Xie, and F.-S. Zhang, Theoretical study on production of heavy neutron-rich isotopes around the  $N = 126$  shell closure in radioactive beam induced transfer reactions, *Phys. Lett. B* **767**, 437 (2017).
- [38] T. Glasmacher, B. Sherrill, W. Nazarewicz, A. Gade, P. Mantica, J. Wei, G. Bollen, and B. Bull, Facility for rare isotope beams update for nuclear physics news, *Nucl. Phys. News* **27**, 28 (2017).
- [39] H. Sakurai, Nuclear reaction and structure programs at riken, *Nucl. Phys. A* **834**, 388c (2010).
- [40] M. Lewitowicz, The SPIRAL2 project and experiments with high-intensity rare isotope beams, *J. Phys. Conf. Ser.* **312**, 052014 (2011).
- [41] J. Yang, J. Xia, G. Xiao, H. Xu, H. Zhao, X. Zhou, X. Ma, Y. He, L. Ma, D. Gao *et al.*, High intensity heavy ion accelerator facility (HIAF) in China, *Nucl. Instrum. Methods Phys. Res. Sect. B* **317**, 263 (2013).
- [42] L. Zhu, C. Li, J. Su, C.-C. Guo, and W. Hua, Advantages of the multinucleon transfer reactions based on  $^{238}\text{U}$  target for producing neutron-rich isotopes around  $N = 126$ , *Phys. Lett. B* **791**, 20 (2019).
- [43] L. Zhu, Shell inhibition on production of  $N = 126$  isotones in multinucleon transfer reactions, *Phys. Lett. B* **816**, 136226 (2021).
- [44] L. Zhu and J. Su, Unified description of fusion and multinucleon transfer processes within the dinuclear system model, *Phys. Rev. C* **104**, 044606 (2021).
- [45] J. Q. Li and G. Wolschin, Distribution of the dissipated angular momentum in heavy-ion collisions, *Phys. Rev. C* **27**, 590 (1983).
- [46] G. Wolschin and W. Nörenberg, Analysis of relaxation phenomena in heavy-ion collisions, *Z. Phys. A: At. Nucl.* **284**, 209 (1978).
- [47] L. Zhu, J. Su, P.-W. Wen, C.-C. Guo, and C. Li, Multinucleon transfer process in the reaction  $^{160}\text{Gd} + ^{186}\text{W}$ , *Phys. Rev. C* **98**, 034609 (2018).
- [48] S. Ayik, B. Schürmann, and W. Nörenberg, Microscopic transport theory of heavy-ion collisions, *Z. Phys. A: At. Nucl.* **277**, 299 (1976).
- [49] W. Nörenberg, Quantum-statistical approach to gross properties of peripheral collisions between heavy nuclei, *Z. Phys. A: At. Nucl.* **274**, 241 (1975).
- [50] L. Zhu, P.-W. Wen, C.-J. Lin, X.-J. Bao, J. Su, C. Li, and C.-C. Guo, Shell effects in a multinucleon transfer process, *Phys. Rev. C* **97**, 044614 (2018).
- [51] V. Zagrebaev and W. Greiner, Shell effects in damped collisions: A new way to superheavies, *J. Phys. G: Nucl. Part. Phys.* **34**, 2265 (2007).
- [52] G. Adamian, N. Antonenko, R. Jolos, S. Ivanova, and O. Melnikova, Effective nucleus-nucleus potential for calculation of potential energy of a dinuclear system, *Int. J. Mod. Phys. E* **05**, 191 (1996).
- [53] C. Wong, Interaction Barrier in Charged-Particle Nuclear Reactions, *Phys. Rev. Lett.* **31**, 766 (1973).
- [54] N. Wang, Z. Li, and X. Wu, Improved quantum molecular dynamics model and its applications to fusion reaction near barrier, *Phys. Rev. C* **65**, 064608 (2002).
- [55] J. Aichelin, “Quantum” molecular dynamics—a dynamical microscopic  $n$ -body approach to investigate fragment formation and the nuclear equation of state in heavy ion collisions, *Phys. Rep.* **202**, 233 (1991).
- [56] M. Papa, T. Maruyama, and A. Bonasera, Constrained molecular dynamics approach to fermionic systems, *Phys. Rev. C* **64**, 024612 (2001).
- [57] C. Li, J. Tian, and F.-S. Zhang, Production mechanism of the neutron-rich nuclei in multinucleon transfer reactions: A reaction time scale analysis in energy dissipation process, *Phys. Lett. B* **809**, 135697 (2020).
- [58] C. Li, P. Wen, J. Li, G. Zhang, B. Li, X. Xu, Z. Liu, S. Zhu, and F.-S. Zhang, Production mechanism of new neutron-rich heavy nuclei in the  $^{136}\text{Xe} + ^{198}\text{Pt}$  reaction, *Phys. Lett. B* **776**, 278 (2018).
- [59] R. Charity, M. McMahan, G. Wozniak, R. McDonald, L. Moretto, D. Sarantites, L. Sobotka, G. Guarino, A. Pantaleo, L. Fiore *et al.*, Systematics of complex fragment emission in niobium-induced reactions, *Nucl. Phys. A* **483**, 371 (1988).
- [60] H. Freiesleben and J.-V. Kratz, NZ-equilibration and nucleon exchange in dissipative heavy-ion collisions, *Phys. Rep.* **106**, 1 (1984).
- [61] K. Rehm, H. Essel, K. Hartel, P. Kienle, H. Körner, R. Segel, P. Sperr, and W. Wagner, Time scales for charge equilibration in heavy ion collisions, *Z. Phys. A: At. Nucl.* **293**, 119 (1979).
- [62] R. Donangelo and S. Souza, Charge equilibration in heavy-ion reactions at intermediate energies, *Phys. Lett. B* **409**, 58 (1997).
- [63] G. A. Souliotis, P. N. Fountas, M. Veselsky, S. Galanopoulos, Z. Kohley, A. McIntosh, S. J. Yennello, and A. Bonasera, Isoscaling of heavy projectile residues and  $N/Z$  equilibration in peripheral heavy-ion collisions below the Fermi energy, *Phys. Rev. C* **90**, 064612 (2014).